

Cassegrain ADC: Optical Design Report

Andrew Phillips, UCO/Lick Observatory

Version: Oct 03, 2003

1. Introduction

We have explored and adopted a near-optimum design for the Cassegrain ADC based on the Linear ADC design. The full-up system has been modeled using ZEMAX in three modes: ideal system (to explore the properties of the linear ADC), images formed at the slitmask surface and direct imaging at the LRIS focal surface in both red and blue beams.

Summary of designed linear ADC:

Prism opening angle	2.5°
Prism central thickness	45 mm
Prism clear aperture	1022.2 mm (min.) + 10 mm for safety
First prism offset	-22.1 mm (below center)
Minimum prism edge thickness	22 mm
First prism angle at outer surface	1.67°
First prism angle at inner surface	-0.83°
Minimum prism separation	20 mm
Maximum prism separation	1700 mm
Location in front of telescope focal surface	1695 mm – center of ADC 800 mm – min. distance (wrt 2 nd prism)
Zenith distance for full correction	0 -- 60°
Prism Material	Fused Silica (Grade D suggested)
Coatings	MgF ₂ + Sol-Gel
Expected Transmission	> 94%

Tolerances:

Tolerance in prism position, axial	10 mm
Tolerance in prism position, radial	<5mm (set by safety margin above)
Tolerance in prism angle	0.2°
Tolerance in index inhomogeneity	3×10^{-5}

The nominal plate scale at the Keck focus is 1.379"/mm.

2. Linear ADC, General Properties

The adopted ADC design consists of matched prisms, which are separated to compensate for the changing atmospheric dispersion. This design has the advantage of a single glass type, and for which we have chosen fused Silica for its broad range of transmission. The adopted prism angle is 2.5° with a total path through the glass of 90-mm. The first surface of the prism is tilted slightly (1.67°) with respect to the optical axis of the

telescope in order to optimize image size on the slitmask over the whole Cassegrain field (see below). The maximum separation of the prisms is 1700-mm; the minimum is 20-mm. The orientation of the prisms is fixed with respect to the parallactic angle and thus is fixed in altazimuth telescopes.

The linear ADC works by displacing the focal surface; the amount of displacement depends linearly on the prism separation and the blue are displaced slightly more than the red images, which allows us to largely correct the atmospheric dispersion. However, the dominant effect of the linear ADC is the gross displacement of the focal surface as the prisms separate, shown schematically in Figure 1:

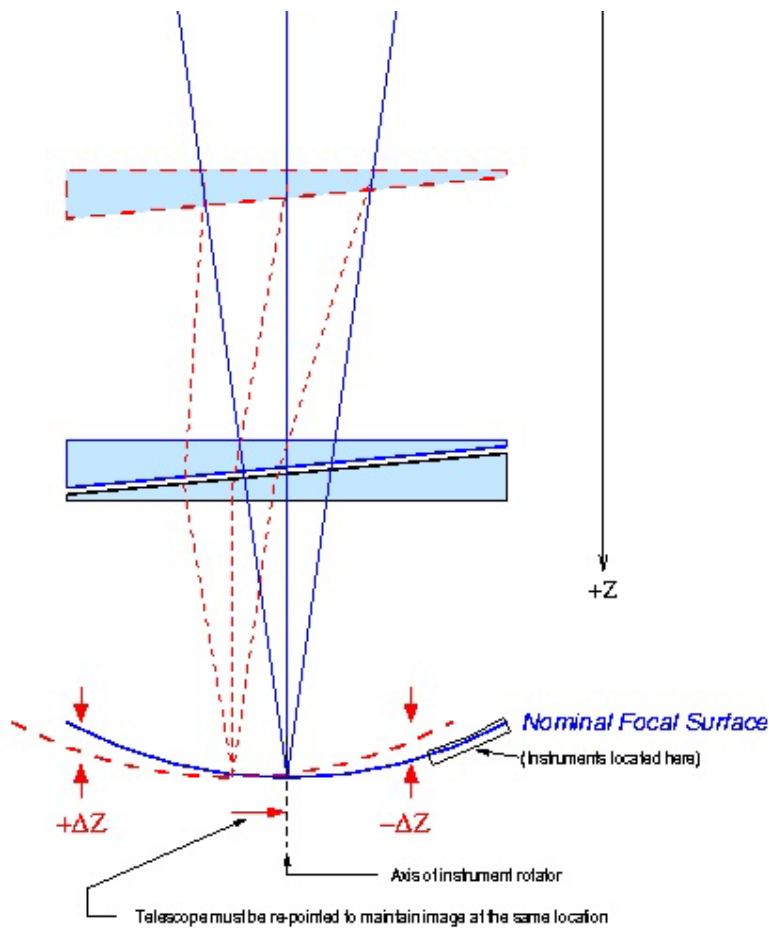


Figure 1: As the prisms separate, the focal surface displaces. For a curved focal surface, this introduces an effective tilt, which must be removed by re-focusing the telescope.

This has several ramifications:

1. The telescope must be continually re-pointed as the prisms change separation (this will occur naturally using the guider); at maximum separation this displacement is 49 arcseconds.

2. The LRIS field is centered approximately 7-arcminutes off-axis. With LRIS located above the horizontal, the focal surface is displaced such that the LRIS field becomes more off axis; below the horizontal the field becomes less off-axis. As the telescope has astigmatic images which become rapidly worse off-axis, this effect means image quality differs both as a function of prism separation and physical angle of LRIS.
3. The Keck focal surface is curved; as it is displaced the focal surface effectively tilts with respect to the non-displaced surface. The gross consequence is that the telescope must be continually refocused as a function of prism separation; however, the tilt across the LRIS field cannot be removed and this affects image quality as well.
4. The LRIS field extends beyond the 10-arcminute radius at which the secondary starts to vignette the field. Thus, as the prisms separate, the displacement means flat-fielding will become less effective. This is a case where the observer may want to select a fixed prism separation, and obtain flat-fields with that separation.
5. The displaced focal surface means that rays entering a particular point in the telescope focal surface will have slightly different angles compared to the non-displaced case. This again means that vignetting within LRIS will be affected, and it raises the possibility of additional sources of vignetting – particularly at the grating. However, the ZEMAX models reveal that the footprint of the pupil image (barely) lands entirely on the grating when the ADC is fully extended.
6. Finally, when the prisms are separated, the locus of beams that can reach the LRIS field (all LRIS orientations) is centered slightly below the optical axis of the telescope. Thus, a circular prism of minimum size will be displaced somewhat below the optical axis. The second prism is centered with respect to LRIS. Ideally, the first prism should be centered in the null position and displace downward as the prisms separate; in practice, we oversize the prism and select a fixed decenter.

We took the opportunity of using the ZEMAX optical model of the Keck telescope plus ADC to check the focal-surface displacement/tilt, using the real system model at full prism separation, and either solving for a tilt in the focal surface or solving for a displacement of the curved focal surface. Results are shown in Fig. 2. While the offset or corresponding tilt is not quite as large as might be predicted, it is obviously present, confirming what we expected.

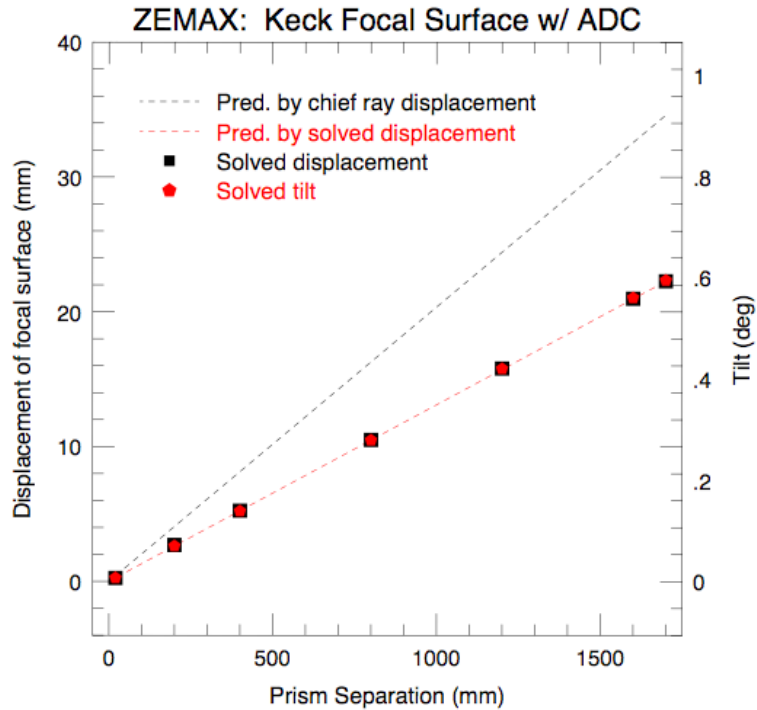


Figure 2: ZEMAX solutions for focal surface tilt/displacement at full prism separation.

3. Ideal System: Aberrations of the ADC Itself

We examined the aberrations introduced by the adopted linear ADC design using an ideal “paraxial” lens of focal length 149.5-m to replace the telescope. This produces point images on a flat focal surface without the ADC in place. The designed closed ADC was placed in the beam with front surface either perpendicular to the optical axis or tilted at the optimum angle; then the ADC was opened to the full 1700-mm separation. In each configuration the ZEMAX ray-fan plots were examined to determine the maximum ray deviation and dominant aberrations:

<i>Description</i>	<i>Prism tilt</i>	<i>Prism sep.</i>	<i>Max. image aberration</i>	<i>RMS radius</i>	<i>Dominant aberration</i>
No ADC	-	-	0	0	-
Closed, untilted ADC	0	0	0.5 μm	<0.2 μm	Spherical
Closed, opt-tilt ADC	1.67°	0	~3	~0.7	Lateral Coma
Closed, Design ADC	1.67°	20 mm	~6	~1.5	Lateral Coma
Fully Open, Design ADC	1.67°	1700 mm	~140	~38	Lateral Coma

(For comparison, the Keck telescope aberrations – dominated by astigmatism -- range from ~85- μm at 4-arcminutes to ~350- μm at 10-arcminutes.)

From this we see that the closed ADC should have virtually no effect on image quality, and images should degrade as the prisms separate. The dominant aberration of the telescope is astigmatism. Images at the focal surface will thus be degraded by a combination of astigmatism (from the telescope), lateral coma (ADC) and defocus (from the tilted focal surface).

No change in plate scale was seen in the different configurations (N.B. this will not be true of the real system in practice).

4. Residual Dispersion

We used ZEMAX to verify the residual dispersion using the ideal system above for simplicity. The residual dispersion is a function of how well the index of refraction of fused silica matches that of the atmosphere. At 60°, 1700-mm prism separation, the residuals for the extreme wavelengths are shown in the table below and Figure 3:

Wavelength	Residual	Residual
0.31 μm	-60 μm	-0.083"
0.59	55	0.076
1.10	-101	-0.139

The dispersion correction is linearly proportional to the prism separation, so the residual at any other prism separation will scale linearly relative to the full separation values above.

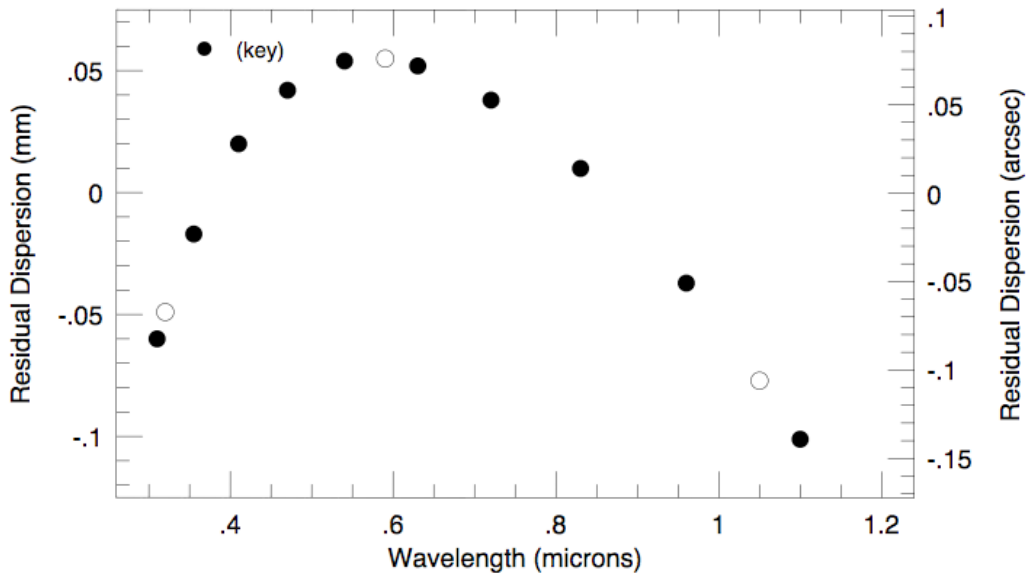


Figure 3: Residual dispersion at full 1700mm separation; rms residual is 0.053".

We find that the residuals of the images at extreme wavelengths, 0.31 and 1.1- μm , vary by $\pm 22\text{-}\mu\text{m}$ and $\pm 10\text{-}\mu\text{m}$ (or ± 0.030 and ± 0.013 arcseconds), respectively, as the prisms separation is varied by $\pm 20\text{-mm}$. This is deemed an acceptable error, so that the tolerance in z-position for a single prism is $\pm 10\text{-mm}$. This is an extremely loose tolerance; we expect to be able to position the prisms to within 1mm at all times.

5. Clear aperture

The clear aperture of the ADC was determined at the extreme points in the LRIS field; the extreme corner of the guider field was not considered and vignetting was expected to occur. Due to the displacement of the focal surface and subsequent repointing of the telescope, the first prism is displaced somewhat from the optical axis of the telescope. Also in determining the clear aperture, it must be remembered that the footprint of the ray bundles on the first prism surface may be dispersed and therefore may be larger than in the monochromatic case.

We used ZEMAX with wavelengths of 0.31 and 1.05 μm (limiting cases) to determine the minimum clear aperture and the decenter required for this aperture. The limiting cases are (1) the LRIS field located at the top of its rotation and the prisms closed (nulled out), and (2) the LRIS field located at the bottom with the prisms fully separated. By examining the required radii in each position as a function of the first prism displacement, a minimum clear aperture of 511.1-mm (radius) with a displacement of -22.1-mm was found. The clear aperture of the second prism was confirmed to be smaller than this, but was not examined in detail as we expect the prisms to be of equal diameter.

6. Image Quality at the Slitmask & Optimum Prism Specs

It is important that the telescope+ADC produces the smallest images at the slitmask surface for optimum spectroscopic performance. Thus, we have performed optimization at the telescope focus on the tilted cylindrical surface representing the slitmask. The only parameters to vary are the tilt of the prisms.

Field Orientations and Field Points:

Since the ADC has a natural axis of symmetry aligned with the parallactic angle, whereas the rotator angle of LRIS is arbitrary, we must choose fields that are sufficiently representative and properly average these. In practice, we have generally used five orientations labeled 1-5 (with the LRIS field centered at 0, 45, 90, 135 and 180 degrees with respect to the vertical, respectively; see Figure 4), although in practice fields 2 and 4 are sufficient to adequately describe image quality. Within each orientation, nine field positions were defined at 4, 7 and 10 arcminutes along the centerline of the LRIS field, and the same points offset $\pm 3.6\text{-arcminutes}$ from the centerline. These same field points and orientation were used throughout all analysis of the telescope and LRIS models.

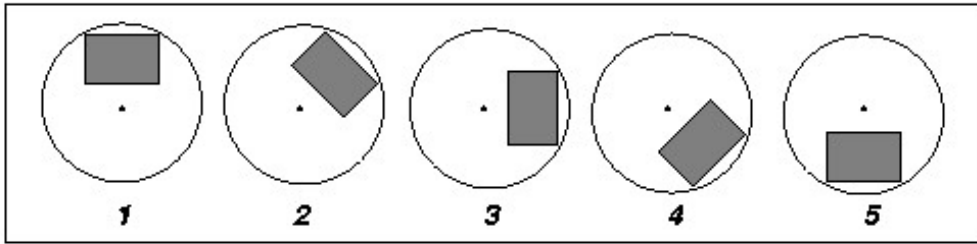


Fig.4

Optimum Prism Angle/Separation:

A range of prism opening angles (5, 2.5 and 1.25 deg) and prism separations was explored; there is a *slight* improvement with smaller prism angles, but the prism separation (and thus clear aperture) must grow correspondingly. For this reason, we adopt the mechanically preferred 2.5° prisms and 1700-mm maximum separation.

Optimum Prism Tilt:

The relative tilt of the prisms with respect to the optical axis affects the image quality, apparently in the play between lateral coma and astigmatism. For each field, we have measured image quality in each of three cases:

1. Using a solved “best” tilt about the X axis;
2. Using a solved “best” tilt about the X and/or Y axis; and
3. Using a fixed tilt (average of Case 1).

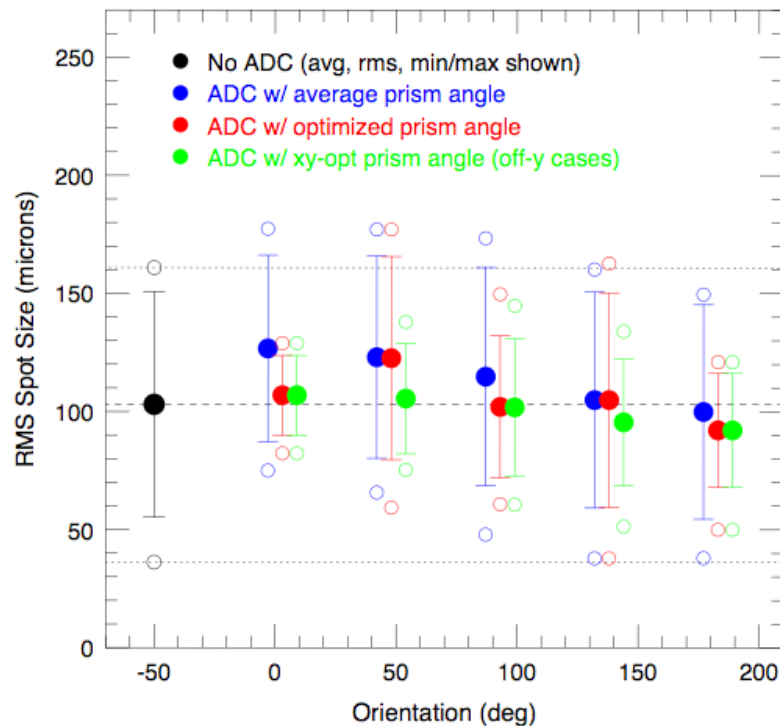


Figure 5: Average, standard deviation (error bars) and extreme image sizes (circles) for Case 1 (red), Case 2 (green) and Case 3 (blue) compared to the non-ADC case (black)

The results are shown graphically in Figure 5. We conclude Cases 1 and 2 are not significantly improved over Case 3 to warrant active control of the prism tilts. The average of the solved tilts is 1.67° at the outer prism surfaces. Figure 5 also demonstrates that better images are obtained in Fields 4 and 5 (when LRIS is below the horizontal) compared to Fields 1 and 2.

Summary of Image Quality Results:

The following table shows the average rms radius for monochromatic images at 0.45- μm for images at the slitmask, for the ADC in “nulled” position (at 20-mm minimum prism separation). Polychromatic wavelengths are 0.31, 0.355, 0.41, 0.47, 0.54, 0.63, 0.77, 0.83, 0.96 and 1.10 μm .

Field	No ADC	ADC nulled, 0.45- μm	ADC nulled, polychromatic *
1 (0°)	$107 \pm 50 \mu\text{m}$	$108 \pm 50 \mu\text{m}$	$110 \pm 50 \mu\text{m}$
2 (45°)	"	108 ± 50	110 ± 50
3 (90°)	"	108 ± 50	109 ± 49
4 (135°)	"	107 ± 50	109 ± 49
5 (180°)	"	107 ± 49	108 ± 49

(* Measurements actually made at 3° zenith distance, which is the minimum corrected distance.)

This table is the same except for the ADC in fully open position, equivalent to full correction at 60° zenith distance:

Field	No ADC (w/o atm. dispersion)	ADC open, 0.45- μm	ADC open, polychromatic
1 (0°)	$107 \pm 50 \mu\text{m}$	$133 \pm 38 \mu\text{m}$	$143 \pm 37 \mu\text{m}$
2 (45°)	"	129 ± 43	140 ± 39
3 (90°)	"	120 ± 48	132 ± 43
4 (135°)	"	113 ± 51	126 ± 45
5 (180°)	"	110 ± 51	124 ± 45

Corresponding FWHM values may be estimated by:

$$FWHM(") = R(\mu\text{m}) \times 2.35 / \sqrt{2} / 725 = 0.0023 \cdot R(\mu\text{m})$$

The worst polychromatic images at the slitmask are approximately 192- μm radius, corresponding to 0.44-arcsec; within the 20-arcmin FOV, the worst are 174- μm radius (0.40-arcsec). These compare to a native images (no ADC) of 168- μm and 149- μm (0.38 and 0.34 arcsec), respectively.

7. Plate Scale and Distortion

While the ideal system shows no change in plate scale, this is not true of the real system, where the effective focal length changes as the system is refocused with the ADC in place. Using the curved Keck focal surface, the effective focal length for the system without ADC was 149587-mm, whereas with the ADC it was 149369-mm (ADC nulled) and 149377-mm (ADC fully open). From this, we find an average change in plate scale of 0.99857 with the ADC. This level of plate scale change produces an error of about 0.33-arcseconds (center-to-edge) over the LRIS field and thus is too large to neglect. In practice, it means observers will need to design slitmasks specific for use with or without the ADC.

Removing the plate scale, the following distortions are found across the fields compared to the no-ADC case:

Field	Closed ADC Rms (rms-x)	Closed ADC Max-x, max-y	Open ADC Rms (rms-x)	Open ADC Max-x, max-y
1	11- μ m (8)	16- μ m, 11- μ m	50- μ m (49)	62- μ m, 22
2	10 (8)	14 7	47 (38)	50 48
3	15 (13)	17 13	36 (12)	17 46
4	11 (9)	15 8	31 (20)	28 37
5	12 (9)	15 14	31 (30)	44 12

For spectroscopy, we are much less concerned with distortion in y (along the slit) than we are with x (across the slit). For the closed ADC, distortion in x is always at or below 17- μ m (0.023") for the closed ADC, which is negligible. For the open ADC, the maximum distortion in x is 62- μ m (0.086"), which is becoming significant, although with LRIS below the horizontal as recommended, this maximum deviation is only 44- μ m (0.061"), which is more acceptable.

8. Images at LRIS Focal Plane

The entire system with both Red and Blue LRIS paths has been modeled.

Some notes on the LRIS ZEMAX models:

1. The aperture at the field lens has been increased ± 2.5 -mm in Y in order to avoid vignetting the inner field rays (the field points had been previously defined and thus it was easier to increase the aperture than redefine the points).
2. The Red camera was modified to have the correct aspheric surfaces, and to use the as-built radii and spacings (courtesy of Harland Epps); however, the index values are standard rather than specific melt values. The model of the Red camera was tested alone in collimated light and found to match the performance predicted by Epps.

3. The Blue camera model is based on the Blue-side ZEMAX model from CARA updated with as-built 2C parameters (including indices) from a Code V model provided by Chuck Steidel. The performance of the Blue side matches the image sizes found by Steidel (25- μm FWHM images of slitmask pinholes).

Results:

The following table gives the polychromatic image size (rms radius in microns):

Camera	Field	No ADC	ADC nulled	ADC open
Blue *	2	17.0 \pm 2.1 μm	17.6 \pm 1.9 μm	20.2 \pm 4.2 μm
Blue *	4	"	17.3 \pm 2.1	18.0 \pm 1.9
Red **	2	25.8 \pm 6.6	26.1 \pm 6.6	27.7 \pm 6.3
Red **	4	"	25.9 \pm 7.2	29.4 \pm 7.7

(* Wavelengths used for Blue camera were 0.31, 0.37, 0.43, 0.49 and 0.55 μm .)

(** Wavelengths used for Red camera were 0.45, 0.54, 0.64, 0.77, 0.92 and 1.10 μm .)

The worst LRIS-R images seen at the 10-arcmin field point have a radius of 38.0- μm , or about 0.55-arcsec (vs the no-ADC case of 33- μm or 0.49-arcsec).

9. Materials

Glass:

The glass is fused silica, chosen for its transparency over the required wavelength range, 0.31- μm to 1.05- μm .

Index of Refraction Inhomogeneities:

The effect of index inhomogeneity is negligible for the grade of fused silica selected (Grade D). The worst case is for an inhomogeneity to occur in Prism 1 at maximum separation. The displacement of a ray passing through an inhomogeneity, ϵn , is easily calculated from the thin-prism approximation,

$$\theta = (n - 1)\alpha$$

The total angular displacement is

$$\Delta\theta = \theta_1 + \theta_2 = \alpha(n_1 - n_2) = \alpha\epsilon n$$

and the total lateral displacement is then

$$\Delta x = D\alpha\epsilon n$$

where D is the total distance from Prism 1 to the focal plane. For values of $D = 2.59\text{-m}$ (worst case), $\alpha = 2.5^\circ$ and $n = 1.5$, we find a lateral displacement $\Delta x = 0.5\mu\text{m}$ for $\epsilon = 3 \times 10^{-6}$, corresponding to Grade D glass. Since typical rms radii of images are of order 100 μm , the ray displacement due to index inhomogeneities of this size will have

negligible impact on image quality. If we adopt 5- μm as the acceptable limit, we find the index homogeneity should be better than 3×10^{-5} .

Athermalization:

We find a 5C temperature difference results in an index change of $\leq 5 \times 10^{-5}$. Thus, if there were a 5C temperature differential within a beam footprint at the prism, we would see (following the argument above) up to 8- μm ray deflection. As this deflection is small and the scenario described is extreme, athermalization should be insignificant from an optical perspective.

Prism Sag:

The prisms are large lenses supported at their edges, and sag may be a concern (although refraction by thin prisms are not particularly sensitive to small angle perturbations). To explore the effects, we note that in any portion of a prism, sag would be equivalent to an independent tilt of that particular portion relative to the whole – so we can note the magnitude of image displacement as we tilt the entire prism as representative of the distortion that could be introduced by a sagging portion of the prism. The worst case will occur with a tilt of the first prism at maximum separation, as this has the largest pathlength to the focal plan. A tilt of 0.03° , equivalent to about 270- μm sag at the center of the prism, gives image motion of 7- μm at the telescope focus, which is insignificant. The actual estimated sag is 24- μm at the zenith (when the prisms would be closed, not extended), and any sag will be partially countered by sag in the second prism, so sag is not a concern.

Mechanical Tolerances:

Since the prisms have no optical power, radial displacements have virtually no effect. Thus, the tolerance to radial displacement is set entirely by the safety margin around the clear aperture. The angular tolerance is set by a degree of introduced distortion as the two prism angles lose their complementarity. An angle of 0.2° added to the first prism results in distortions of order $\pm 15\text{-}20\text{-}\mu\text{m}$ in the telescope focal plane, which is acceptable but significant. Therefore, 0.2° is a reasonable tolerance for the prism angle mismatch.

Transmission:

(Adapted from the Conceptual Design Review:)

Using the coatings described below (4 surfaces) and 90mm of high-grade Silica, throughput should be above 94% at all wavelengths 0.31—1.05- μm .

The total throughput of the glass (90mm of HPFS 7980) and AR coatings (measured GMOS values above 0.4- μm and assuming 0.99 for a single coating or 0.96 for 4 surfaces for the UV below 0.4- μm) gives:

<i>Wavelength (microns)</i>	<i>Estimated Total Throughput</i>
0.30	0.943
0.32	0.948

0.35	0.956
0.40	0.960
0.45	0.974
0.55	0.971
0.65	0.982
0.75	0.990
0.80	0.992
0.90	0.987
0.93	0.964
1.00	0.988
1.10	0.970

Coatings:

We will coat the four surfaces with MgF₂ and Sol-Gel, with an expected transmission of 99% or better for each surface. We anticipate the MgF₂ coating will be applied at UCO/Lick and the Sol-Gel applied at LNL. Specifications of the thickness of each layer have not yet been calculated.

We have visited the LNL facility for a tour and to confirm that their largest tank is capable of coating prisms of the required diameter (UCO/Lick shops would need to construct the necessary harness). Furthermore, after discussions with James Stilburn (DOA) and Ian Thomas (LNL), we have determined that UCO/Lick Instrument Shops should develop the equipment necessary to apply these coatings; thus there is a fall-back position of applying the Sol-Gel in house, although timescales for this are TBD.

Furthermore, UCO/Lick is currently modifying a vacuum coatings chamber capable of holding the prisms for the MgF₂ coating, or the coating could be applied in the Mt. Hamilton vacuum chamber. Cleaner MgF₂ coatings are also available (at a higher cost) from outside vendors.

10. Ghosting

At Conceptual Design Review, it was noted that the worst ghosting within the ADC was due to the inner prism faces, and would be worst when the prisms were closest. At these parallel surfaces, we expect ghosts at the integrated level of 0.01% (that is, 1% reflection at each surface), with the light spread over a defocus spot whose size is set by the separation of the surfaces. For the two inner surfaces at closest separation, this means a spot 40-mm out-of-focus, or 2-arcsec in diameter. The quantitative effect of this depends on the PSF of the source. As an example, a stellar Moffat profile PSF with 0.5" FWHM convolved with a top-hat function of 2" diameter has a peak ghost intensity of 3.3×10^{-6} , and the ghost is everywhere $< 3.4 \times 10^{-3}$ below the level of the wings; the maximum ratio occurs at a radius of 2.0" from the star. (For a Gaussian profile of the same width, the

maximum ghost intensity is also 3.3×10^{-6} of the PSF peak, but the ghost sometimes exceeds the intensity of the wings. For a 1.0" Gaussian profile, the peak ghost intensity is 9.1×10^{-6} .) As the prisms separate, the area of the ghost increases as $(\Delta z)^2$ while the intensity falls inversely with the area. The ghost image will be slightly decentered with respect to the primary image; the worst case is at 10-arcmin from the telescope axis with the inner surface tilts adding to the angle, in which case a decenter of 2.1" (at 20-mm prism separation) is possible. The average decenter is 0.9" at closed position. The decenter increases linearly with prism separation.

Other potential sources of ghosts are:

1. reflections coming back through the instrument (but these will be defocused by twice the distance from the telescope focus to the prisms (that is, defocused by more than 1600mm); or
2. reflection off the LRIS field lens (but these lens surfaces, located just 76—90mm behind the focus, produce divergent rather than convergent reflected rays); or
3. reflections off the slitmask, which could be focused in one axis due to the curvature of the mask; however, the mask is tilted 8.06° , so any rays reflected from this surface will be of order 16° off-axis, and such rays would be outside the aperture created by the grating (and these reflected rays would also be divergent since the slitmask is located so close to the telescope focus).

Thus, we conclude that ghosting from sources outside the ADC are negligible.

11. Guider

The moveable guider field is unvignetted to a radius of 10.8 arcminutes off axis; beyond this, vignetting increases to a maximum loss of ~25—30% (slightly less with the safety margin of the clear aperture). This appears to be fairly uniform at all field orientations and prism separations.

12. Miscellaneous Concerns/Notes

1. The displacement of the field has a serious implication for the pointing model – the location of the Pointing Origin (as referenced to the telescope axis) moves with respect to the LRIS field. This means that the pointing model may need to remove the focal surface displacement before making any pointing calculations. It also means that slitmask alignment must be aware of the (changing) location of the Pointing Origin in the alignment images ... Another way of looking at this is that the rotator axis falls on a different part of the sky than the telescope axis.
2. The telescope focus algorithm will need to adjust focus as a function of elevation (or prism separation) and physical rotator angle. This is related to the focal-surface offset. (This function, as well as that of prism separation as a function of elevation, are TBD, but they are straight forward to determine.)

3. Observers will want to choose PAs so that LRIS is below the horizontal if the best image quality is desired (at least for spectroscopy).
4. The prism separation at a function of elevation may be different depending on the wavelengths of interest, e.g., if the observer is not interested in wavelengths beyond 0.6-um, smaller dispersion residuals can be produced with slightly different prism spacing. This can be easily controlled by a scale factor keyword, where the scale factor is calculated for the wavelength range of interest.
5. Note on ZEMAX models: There seems to be some roundoff problem in ZEMAX related to the entrance pupil diameter vs. primary diameter; the pupil diameter was reduced 0.1-mm to solve this problem.

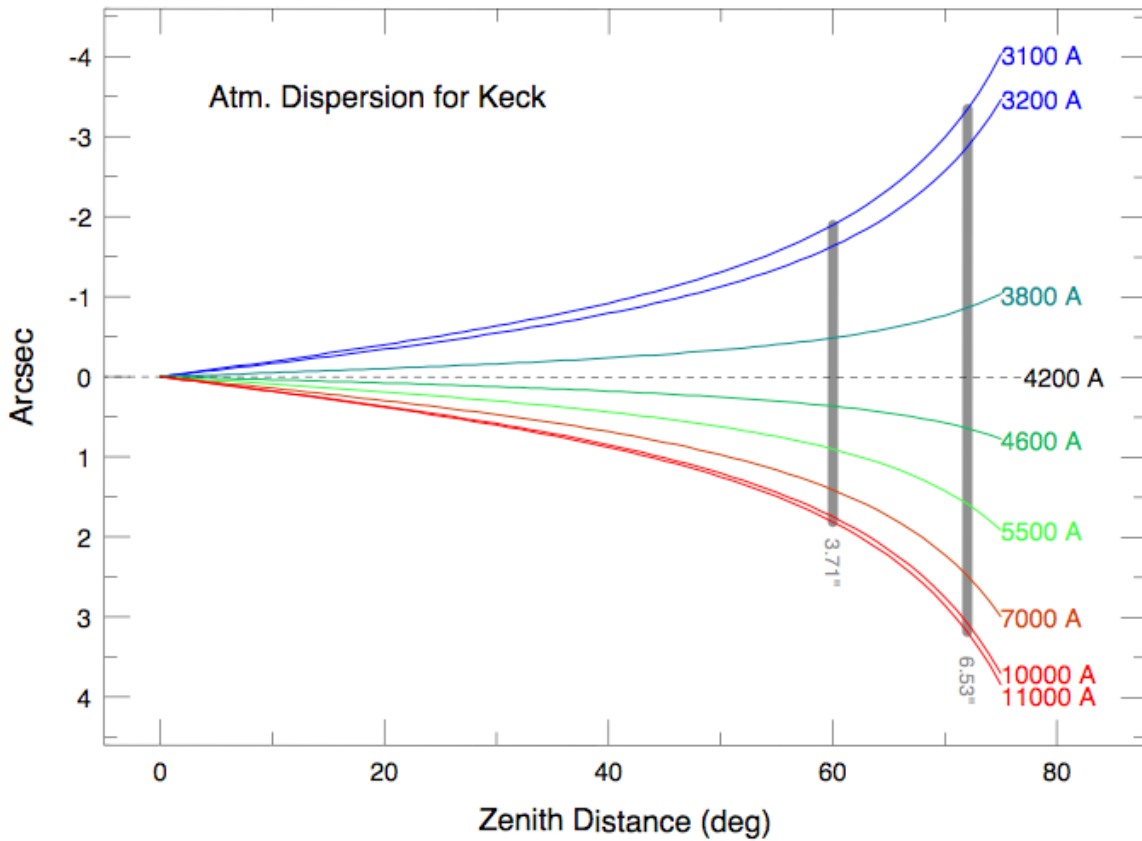


Figure 6: Atmospheric Dispersion at Keck

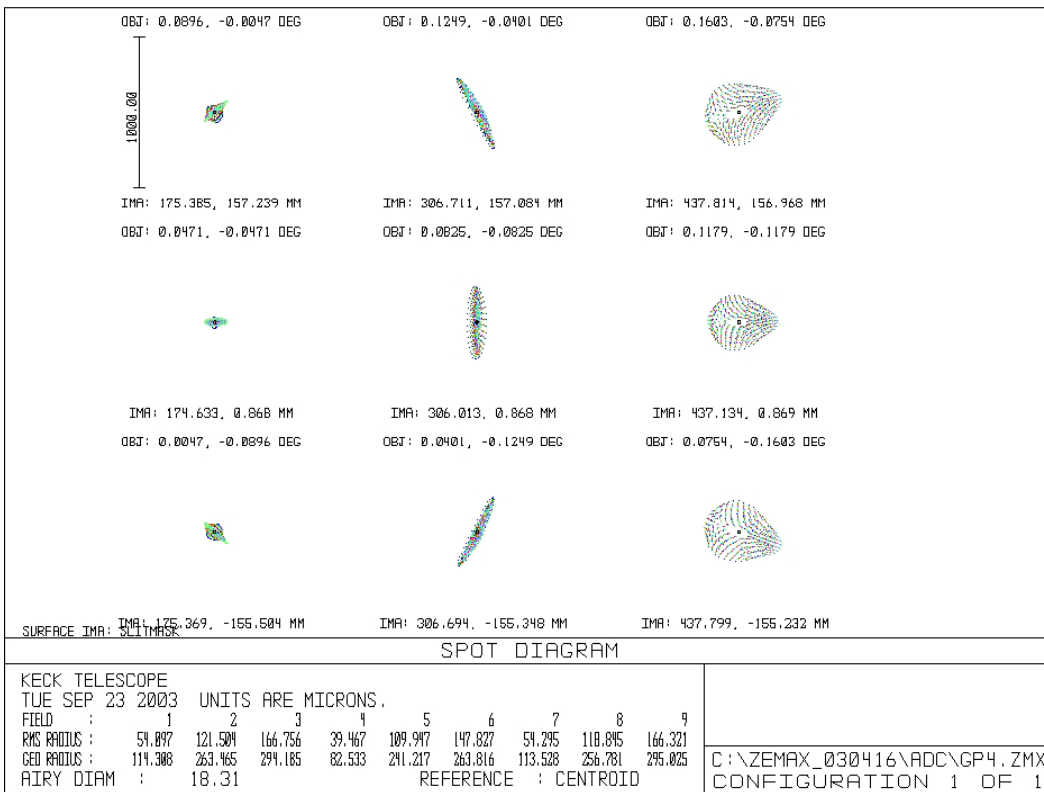
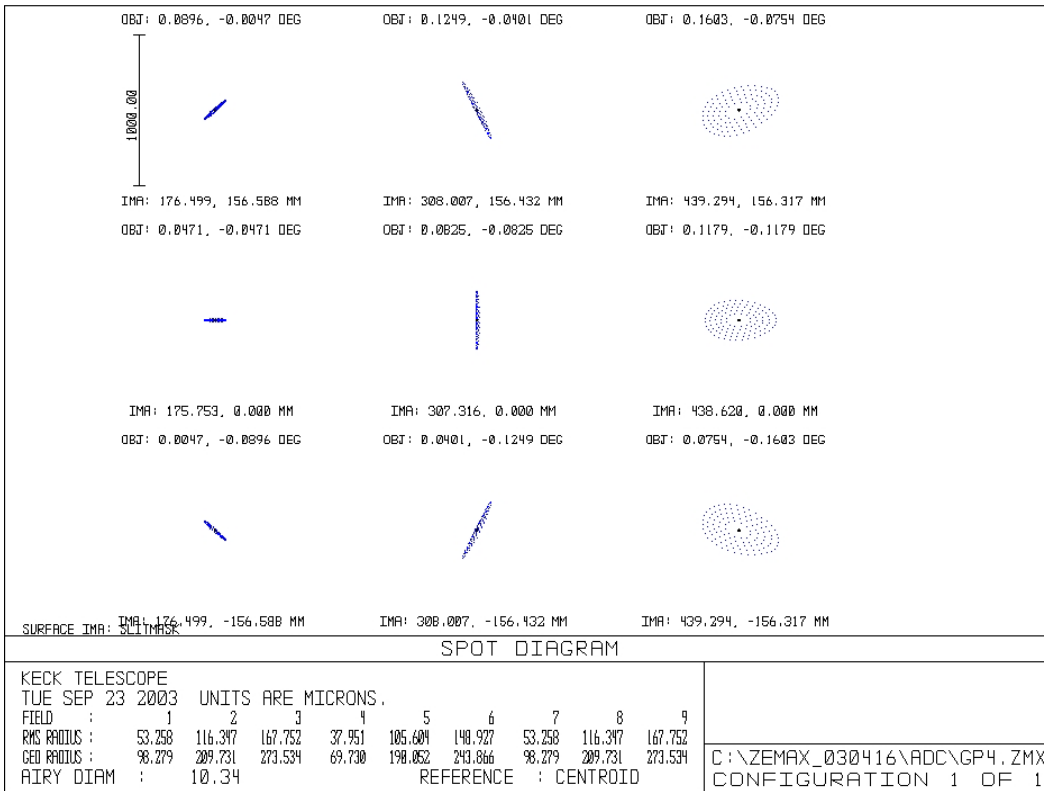


Figure 7: Images at slitmask, zenith -- no ADC (top) and with nulled ADC (bottom).

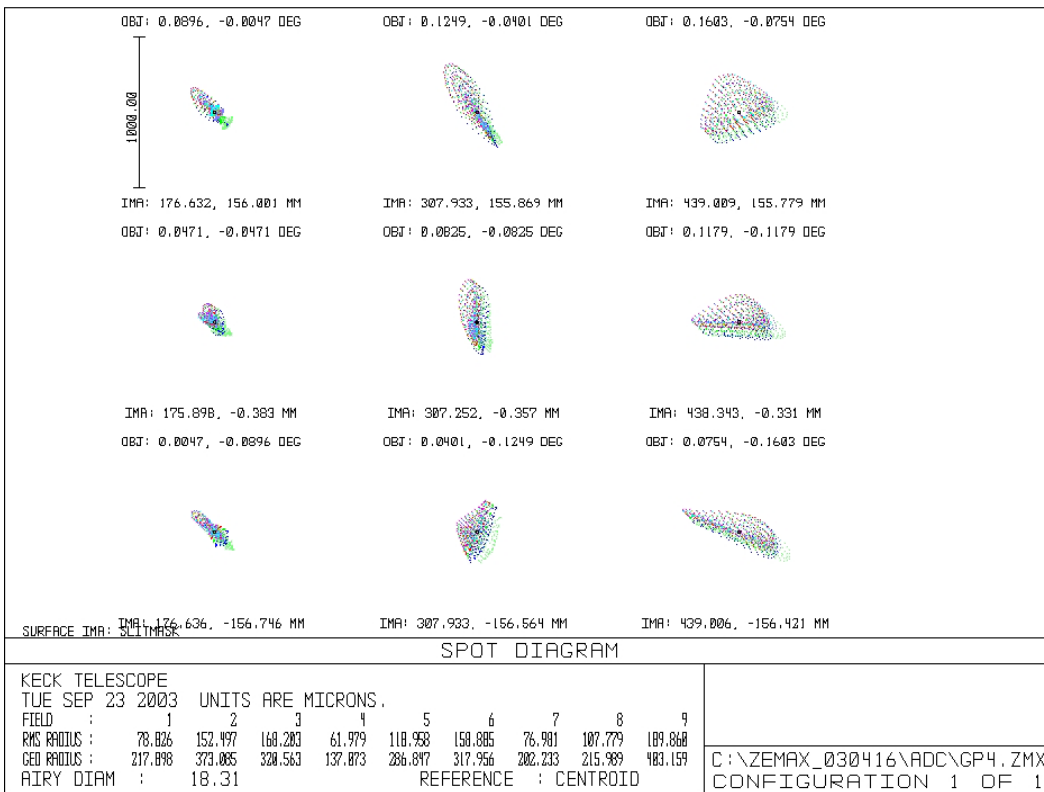
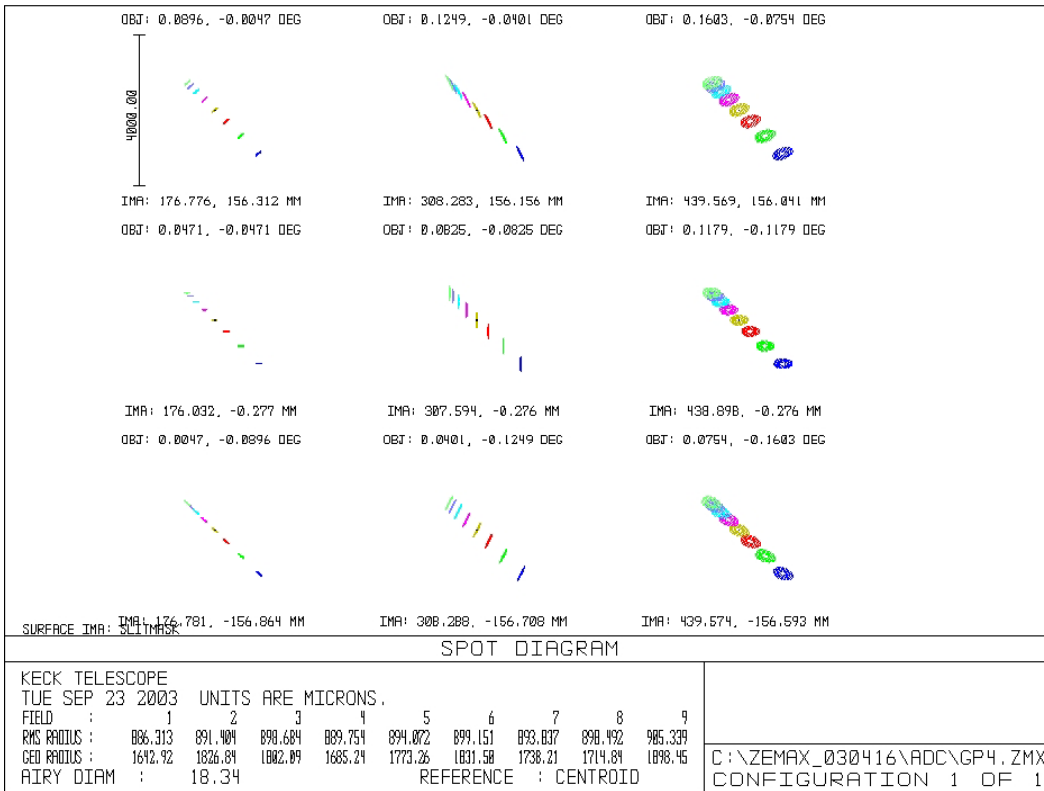


Figure 8: Images at slitmask, $Z=60^\circ$ -- no ADC (top) and with ADC (bottom).

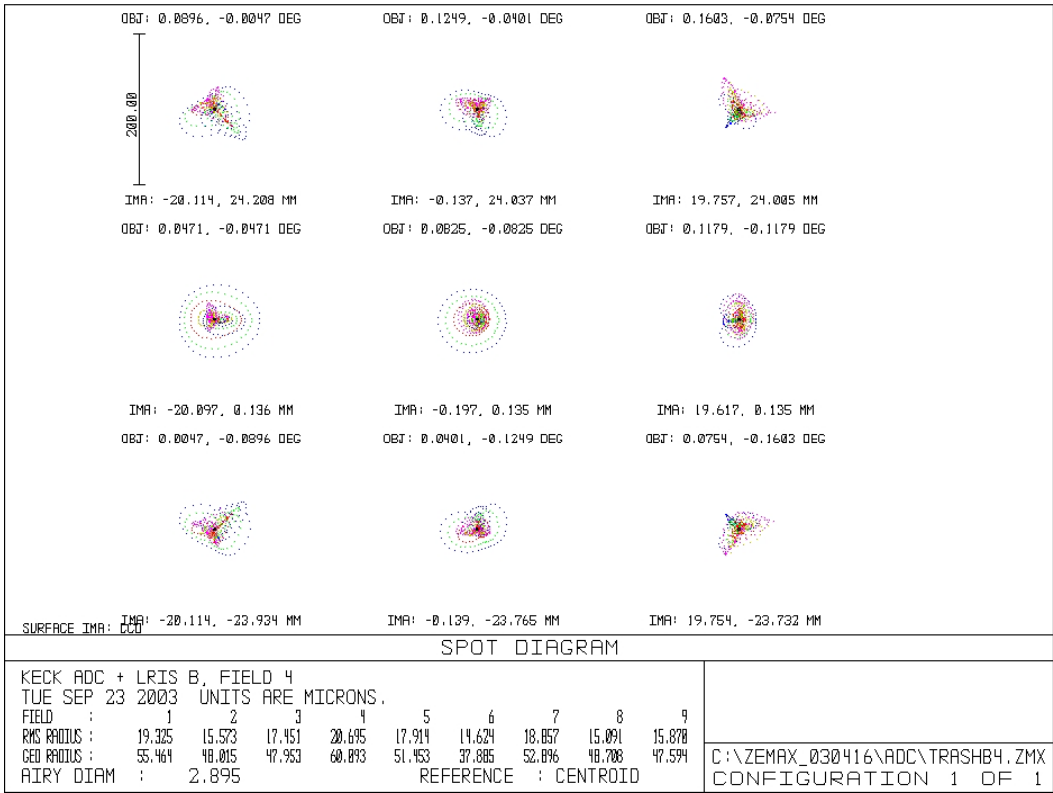
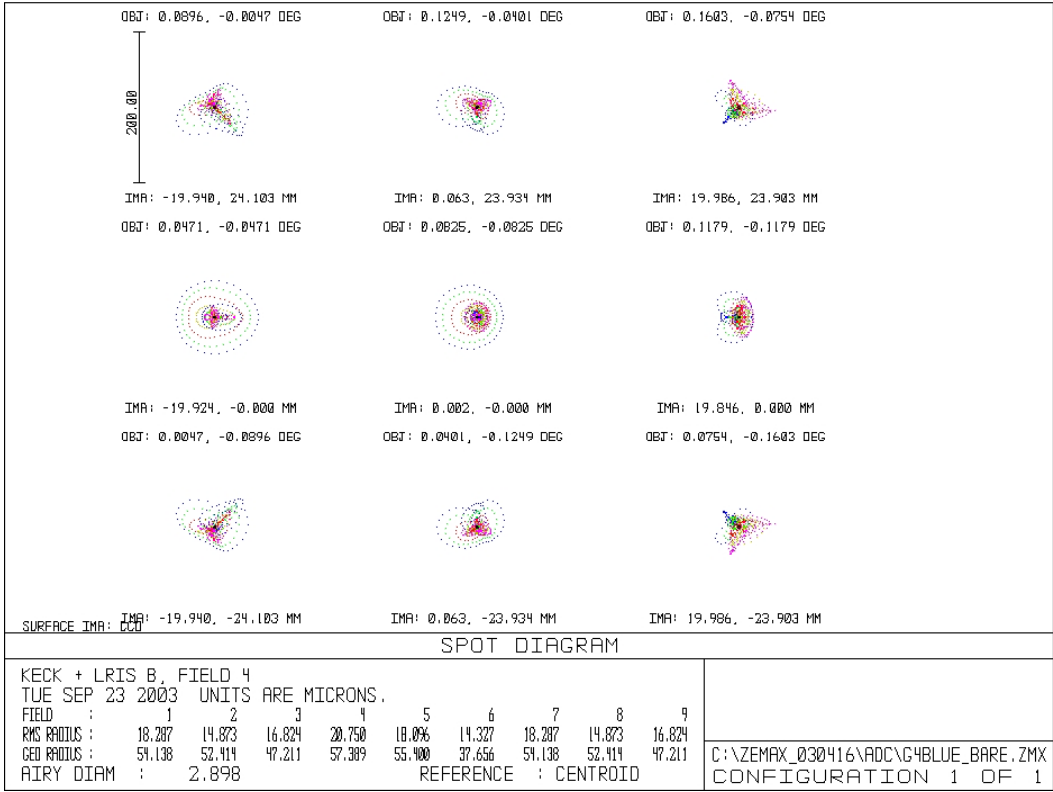


Figure 9: LRIS-B images, $Z=0^\circ$ -- no ADC (top) and nulled ADC (bottom).

13. Alternative Designs

We briefly consider an example of an alternative design that is considerably more difficult and costly to fabricate, and hence was not explored further. The idea is that the ADC prisms surfaces could be designed to overcome some of the aberrations inherent in the RC design of the telescope. Since the dominant telescope aberration is astigmatism, this would involve giving each small portion of the prism an axisymmetric cylindrical component. Clearly, spherical surfaces will not provide this, so the surfaces will be aspheric. Also, there are two immediately apparent constraints:

1. Each prism must have net zero power, or else the effect will be strongly dependent on prism separation. In effect, this means the surfaces must be put on the front and back of a single prism, so that the distance between these powered surfaces is fixed;
2. Since each prism has a variable (non-axisymmetric) thickness, and the power is only working within the prism, axisymmetric surfaces on single prism will be unable to correct the problem, so both prisms must be figured with similar surfaces.

Thus we need four aspheric surfaces. We present below an example design to illustrate the level of improvement in image quality we can expect. This has been modeled using the curved focal surface of the telescope. In order to avoid the complication of the tilted focal surface as the prisms displace the field, we have allowed the second prism and focal surface to displace as the prisms separate and have sampled the entire field simultaneously. The field points are on the x-axis at 0, 0.03, 0.06, 0.09, 0.11667, 0.13, 0.16667, and 0.17 degrees, plus on the y-axis at ± 4 and ± 10 arcminutes. This sampling was chosen to provide a sufficiently high density for testing the aspheric surfaces. (In the optical model with the displaced prism/focal surface, the aberrations show a high degree of radial symmetry, at least in the nulled position.) Note that the models solved for the best asphere parameters in the nulled position only – no balancing was performed to try to obtain the best results across the range of prism separations.

Model	Closed/Nulled rms-Radii (μm)				Open (1700mm) rms-Radii (μm)			
	0	4'	10'	avg	0	4'	10'	avg
No ADC	13	24	145	73 ± 57				
Planar	20	28	145	75 ± 55	68	91	147	96 ± 60
2 nd order asphere	50	39	97	61 ± 27	51	68	195	104 ± 67
3 rd order asphere	56	26	111	63 ± 37	79	82	146	89 ± 43
4 th order asphere	43	33	104	61 ± 33	66	88	164	91 ± 55
4 th + 6 th order	26	36	99	60 ± 31	70	89	145	87 ± 44

The advantage here is probably seen more by examining the 10-arcmin images than in the average, as the inner images (which are very good) degrade somewhat as the outer images (poor) improve. This can be seen in the average with the strong decline in the rms image size along with the more modest decline in the average value. Also, as an ADC is required, the comparison should be made between the planar and aspheric ADC values. (These numbers should only be compared internally – they should *not* be compared with the design ADC numbers for the non-displaced slitmask focus.)

The expense of the aspheres is in three places: (1) additional glass; (2) polishing time in the Lick shops; and (3) tooling fabrication time. Dave Hilyard estimates 20 months for the asphere fabrication and testing (although there may be a time savings in the fact that the four surfaces are identical aspheres). The 4th order and 4+6th order models deviate by about 0.1-mm from planar surfaces, so the added expense is primarily in Lick Shop time.